Asbestos fibers breakdown by Self-sustained High temperature Synthesis - SHS

Gaggero Laura[1], Caratto Valentina[1], Ferretti Maurizio[2]*

[1] Department of Earth, Environment and Life Sciences, University of Genoa, Corso Europa 26, I-16132 Genoa, Italy

[2] Department of Chemistry and Industrial Chemistry, University of Genoa, Via Dodecaneso 31, I-16146 Genoa, Italy

* Correspondig author: ferretti@chimica.unige.it – phone +39 010 3536085

Key words: chrysotile, asbestos, fibers, inertization, combustion synthesis, SHS

Abstract

The SHS technique was experimented in chrysotile breakdown taking advantage of the heat release of the highly exothermic reactions ignited by a relative low energy source. By means of two reactions such as $Mg_3Si_2O_5(OH)_4 + Fe_2O_3 + 3Mg$ and $2Mg_3Si_2O_5(OH)_4 + Fe_3O_4 + 4Mg$ the chrysotile was completely converted into forsterite-rich olivine. Different mixtures of hematite + Mg and magnetite + Mg were tested with chrysotile to establish the maximum chrysotile amount in order to allow the reaction. In comparison with conventional thermal treatments, the SHS process, due to fast reaction time, low activation energy and simple instruments, particularly advantages the asbestos neutralisation, positively reflecting into time and costs of the process. The product of this transformation is liable to be re-used so this represents the end of waste status and a second life as secondary raw material.

1. Introduction

Following the dismissal of asbestos in industrial and civil uses, increasing amounts of fibre-bearing wastes represent a priority alert.

As assessed, the exposure to asbestos has mutagenic effects inducing some asbestos related diseases, in particular malignant mesothelioma [1]. Thus in March 2013 the European Commission has deliberated the resolution 2012/2065(INI) [2] that compels the member states to remove and eliminate all asbestos containing waste within 2028.

Several methods were proposed for the disposal of materials containing asbestos, such as definitive removal, insulation by resin coating and encapsulation [3, 4]. After removal, neutralisation has been proposed by fluorosulphonic acid attack [5], carbonation [6], hydrothermal process [7], thermal treatments [8, 9] and mechano-chemical methods [10, 11]. However, encapsulation and coating are temporary solutions, as the material is still subject to weathering. Moreover, fibre treatments based on chemical attack are liable to release toxic vapours.

Thermal treatments at temperatures above 800° up to 1000°C demonstrate efficient in transforming chrysotile into Mg–silicates [12, 13], although pseudomorphic on the pristine fibrous habit. In fact, the dehydroxilation reaction of chrysotile is characterized by an endothermic step between 600° and 700°C associated with the formation of an amorphous phase (metachrysotile) [14, 15, 16]. Dehydroxilation is meant when OH-, occupying 75% of octahedral sites, are eliminated from the crystal lattice, originating an amorphous phase [14, 17, 18, 19, 20]. In particular at 620°C the neoformed forsterite begins to develop topotactic on the relics of chrysotile structure [18, 19]. At about 800°C a phase transition from metachrysotile to forsterite follows [12, 21]. Ion diffusion determines selective Mg^{2+} and Si^{4+} enrichment [19, 20] in domains where forsterite nucleates first, followed by enstatite at temperature exceeding 1000°C [18]. Quantitative XR diffractometry demonstrated that residual silica from forsterite nucleation reacts with the latter to produce enstatite [21]. Furthermore, as confirmed by NMR spectroscopy [15], IR spectroscopy and TEM imaging and high temperature in situ XRD [12] a multistep dehydroxilation path is inferred.

In the perspective of reducing the environmental issue and to explore possible recycling of the breakdown products of chrysotile, we experimented the use of Self-sustained High-temperature Synthesis (SHS), a non-conventional thermal treatment assessed since the Sixties for the synthesis of ceramic materials [22].

A “thermite” or “aluminothermic” reaction involves the exothermic reduction of a metallic reagent and a metal oxide into an oxide more stable than the pristine. The reaction starts by punctual heating of the mixture until the triggering of the reaction that proceeds as self sustained (hence “Self-sustained High temperature Synthesis).

In order to have a SHS development the “adiabatic” temperature (T_{ad} ≥ 1800 K) [23, 24] has been envisaged as thermodynamic boundary.

The SHS technique was experimented also in waste treatment, with positive results in the fixation and consolidation of high-level radioactive waste, the treatment of zinc hydro-metallurgical waste, the degradation of chlorinated aromatics and the recycling of silicon sludge and aluminium dross produced by the semiconductor industry and aluminium foundries, respectively, and in the treatment of fibrous minerals, with particular attention to sepiolite [25, 26].

2. Experimental

2.1 Materials and methods

In order to evaluate the effectiveness of chrysotile breakdown by self-propagating high-temperature synthesis (SHS), preliminary experiments were carried out by conventional step heating. In both cases the starting reactant was a natural chrysotile from a veined serpentinite in Petronio Valley (Eastern Liguria, Sestri Levante – Genova) [27] (sample Ba230407_6; Figure 1). It was preventively characterized by optical microscopy, XRPD and micro-Raman analysis (Figure 2 a and b). The fibres from the same veins were used for both the conventional step heating and the SHS experiments, in order to guarantee homogeneous starting material.

The composition of Ba230407_6 chrysotile is comparable with those reported in literature [28, 29, 30, 31] (Table 1). Aluminium in the tetrahedral site is absent or very low (Al^{IV} = 0.022 a.p.f.u.) and Mg in the octahedral site is partially replaced by Al (0.035 – 0.086 a.p.f.u.) and Fe (0.088 – 0.126 a.p.f.u.). Manganese and Cr are low (Mn = 0.002 – 0.006 a.p.f.u.; Cr = 0.000 – 0.014 a.p.f.u.), whereas Ni is absent.

The characterization of both reactants and reacted products was carried out by XRP diffractometry and by SEM + EDS.

Micro-Raman spectrometry was carried out on the same textural sites of electron microprobe analyses (EMPA), confirming the characterisation.

Qualitative and quantitative analyses were performed by a transmitted light polarizing microscope equipped with an electronic point counter. Macroscopic fibrous minerals, covering the sample surfaces or filling open fractures, veins, and voids, were sampled by a diamond file, then manually and magnetically separated, and analysed by XRPD, effective for univocal resolution of mineral mixtures. XRPD analyses were carried out using a Philips PW1140-XCHANGE diffractometre (CuKα

radiation; current 30 mA, voltage 40 kV, scan speed, 0.5°2θ/min; scan interval, 3-80° 2θ.) and interfaced with PC-APD software for data acquisition and processing.

Selected samples (very thin veins or tremolite-chrysotile mixtures) were investigated by Philips SEM 515 scanning electron microscope, equipped with an EDAX PV9100 spectrometer in the energy dispersive mode. Operating conditions were 15 kV accelerating voltage and 2.1 nA of beam current. Raw data were reduced using the ZAF algorithm and the standard software of the EDAX PV9100. Further images were obtained by a Tescan Vega 3 LM Scanning Electron Microscope equipped with an Apollo X detector and Microanalysis TEAM EDS System. Microphotographs were acquired on graphite – sputter coated 3D samples under high vacuum conditions with backscattered and secondary detectors. Semi-quantitative electron microprobe analyses of phases were obtained under high-vacuum conditions by use of natural standards. The natural standards were preliminarily analysed by WDS microprobe at University of Modena. The in situ mineralogy of the serpentine phases with microtextural control was obtained by micro-Raman spectrometry carried out by Jobin Yvon LabRam with 632.8 nm laser, at “Centro Interdipartimentale Scansetti”, University of Turin.

2.2 Chrysotile breakdown by conventional step heating

The natural clinochrysotile Ba230407_6 from the Bargonasco quarry was pulverized and divided in four. Each aliquot was weighted before and after the thermal treatment in muffle furnace to verify that the dehydroxilation process, corresponding to weight loss about 12-14 %, was completed.

X-ray powder diffraction (Figure 3) of clinochrysotile Ba230407_6 after heating support a complete dehydroxilation already at 620° and the occurrence of the amorphous phase metachrysotile in accordance with Cattaneo et al. [12]. The chrysotile heated at 1000°C for 24 hours evidence a weight loss about 14.7%, stabilized after 36 (14.7%) and 48 (14.6%) hours. After treatment at 1000°C for more than 36 hours our samples resulted composed by forsterite and enstatite still retaining the fibrous habit.

2.3 Chrysotile breakdown by SHS technique

To obtain chrysotile breakdown, experimental procedures typically referred to the SHS method were adopted, taking advantage of the heat release of the highly exothermic reactions ignited by a relative low energy source.

The reactants were selected between different oxide–metal couples capable to activate the so-called “aluminothermic reaction” and to break down the chrysotile:

$$Fe_2O_3 + 3Mg \rightarrow 3MgO + 2Fe \qquad \Delta H_r = - 983,2 \text{ kJ/mol}$$

$$Fe_3O_4 + 4Mg \rightarrow 4MgO + 3Fe \qquad \Delta H_r = - 1286,3 \text{ kJ/mol}$$

Chrysotile was then mixed with reactants (Fe_2O_3 powder 99.99% Carlo Erba Reagents; Fe_3O_4 powder 99.99% Alfa-Aesar; Mg bar 99.99% Sigma-Aldrich) in stoichiometric amounts, according to the following reactions:

$$Mg_3Si_2O_5(OH)_4 + Fe_2O_3 + 3\ Mg \rightarrow 2\ Mg_2SiO_4 + 2MgO + 2Fe + 2H_2O \qquad (1)$$

$$2Mg_3Si_2O_5(OH)_4 + Fe_3O_4 + 4Mg = 2Mg_2SiO_4 + 2MgSiO_3 + 4MgO + 3Fe + 4H_2O \qquad (2)$$

Both reactions are highly exothermic in spite of heat consumption during the transformation of chrysotile:

$$\Delta H_r(1) = - 852,8 \text{ kJ/mol}$$

$$\Delta H_r(2) = - 1109,0 \text{ kJ/mol}$$

The thermodynamic parameters of reagent and minerals phases are reported in Table 2.

The reactants were mixed together with randomly oriented chrysotile fibres (FIGURE 4) and then pressed into cylindrical pellets. Scanning electron microscope backscattered image allowed defining that fibres were dispersed and their modal content. The image elaboration software Image J defined the morphology and the abundance of fibres. The geometric features of chrysotile bundles are listed in Table 3.

2.4 The SHS experiment

The combustion process was carried out in a stainless reaction chamber closed, in which flows argon at ambient pressure (Figure 5).

The chamber contains a heated basement on which the samples are placed. Before the reaction, the samples undergo pre-heating (T of the heating base 200-

300°C) for a few minutes. During this step any trace of water is eliminated from the reactant mixture and the whole sample is equilibrated towards the T of triggering in order to properly start the combustion; this helps to reduce the dispersion of the reaction heat. The reaction temperature was monitored by using a thermocouple.

A W coil is located 5 mm above the pellets. The reaction is activated by heat induction when the coil is made incandescent (over 2000°C) by a power supply (2.5 V, 85 A) which is switched off after a few seconds, as soon as the reaction is initiated.

Working under argon flow avoids both the oxidation of W coil and of Mg powder, before the reaction occurs; in addition the vapour extraction systems enabled operating under depression.

This apparatus was patented by Gaggero et al. [32].

The milled chrysotile was mixed to reactants according to the proportions calculated for reactions 1) and 2) then pressed (1,5 t/m^2) in cylindrical pellets. Each experiment was repeated several times with pellets of different diameter (10÷13 mm) and height (7÷13 mm) to verify experimental reproducibility.

The first series of samples was prepared by finely mixing chrysotile with reagents to obtain a homogeneous mixture. A second series was prepared by placing alternate layers of chrysotile with layers of reagents. In both cases, the reaction proceeded in a self-propagating modality.

Different mixtures of the hematite + Mg and magnetite + Mg were tested with chrysotile (Table 4). In this way we were able to establish the maximum chrysotile amount to obtain the reaction with SHS mode. Using the reactants of both reactions 1 and 2, the chrysotile was completely converted into forsterite-rich olivine (Figure 6).

Because of large temperature gradients and extremely high heating and cooling rates affecting the reactants during combustion, non-equilibrium phases could develop in the products [23]. The non-equilibrium nature of the process would produce non-stoichiometric or intermediate and metastable phases, as in the case of reaction (4) whose final products detected by XRPD analysis were forsterite, MgO and FeO.

3. Results

After ignition, the average loss of weight of the sample resulted *c.* 4%, that normalized to the per cent of chrysotile in the pellet, corresponds to a variable weight

loss between 10 and 12 %, likely corresponding to the dehydroxilation of chrysotile [15, 33 and references within].

A morphologic, mineralogical and compositional characterization of products on ignited pellets was carried out by scanning electron microscope coupled with EDS microanalysis. After the SHS ignition, the fibrous habit completely disappears and the breakdown of chrysotile originates olivine with prismatic stubby habit as shown in Figure 7 (A to F) and related mineral chemistry in Table 5. Neoformed olivine grows in MgO and Fe matrix. The volatiles developed at advancing combustion induce the swelling of pellets and a vesicular texture. Locally, the escape of volatiles is recorded by a vortex texture (Figure 7C); however this effect is minimized by the input of Ar flow.

The *in situ* composition of neoformed olivine ranges between Fo_{99} and Fo_{90} (homogenously mixed pellets) and between Fo_{98} – Fo_{97} (stratified pellets), both comparable with natural olivine from peridotites (Figure 6 and Table 5).

The fayalite content within olivine grains is variable and generally higher towards the crystal rims or in small grains in contact with metallic iron (Figure 7 E, F), suggesting a relationship with the proximity of Fe_2O_3 in the pellet. In order to test the pervasivity of reaction, XRPD analyses were carried out on “Hem + Mg” pellets after SHS reaction. The results evidence that chrysotile is absent both in homogeneously mixed and in stratified pellets and replaced by forsterite, periclase and Fe, thus confirming the morphological and chemical analysis under the scanning electron microscope.

The chrysotile breakdown reaction by SHS did not produce enstatite nor in Hem + Mg and Mgt + Mg mixtures, in contrast with descriptions from natural systems [34] and from conventional thermal treatment [13, 15, 35].

4. Discussion

The pellet moulding was carried out as homogeneous and stratified. In order to evaluate the effectiveness of the SHS reaction at different chrysotile content, a homogeneous mixture of reactants and chrysotile allowed their close contact and an homogeneous propagation front. In fact the reaction speed was constant.

The stratified pellets provided a successful combustion: they were envisaged in the perspective of industrial scale up, to represent the geometry of interbedded tiles and reagents.

The increase of size of the pellets vs. the demonstrated occurrence of the reaction by microtexture and compositional change suggests that the homogeneous mixture attains to breakdown the highest % of chrysotile. At increasing chrysotile content, decreasing reaction temperatures were recorded in the sample (Figure 8).

The SHS reaction, compared with conventional thermal treatments [13, 14, 15], takes to the complete compositional and morphological break down in a very short time (some seconds for the experiments carried out). In the perspective of industrial scale up, the time length of the process is extremely profitable as for energy input.

Gualtieri et al., [35] propose a high temperature process of chrysotile neutralisation after which neoformed olivine grows pseudomorphic on pristine fibres, thus maintaining an overall asbestiform habit. Conversely, following the SHS treatment, the newly formed olivine developed as granular sturdy crystals (Figure 7).

Discrete olivine grains close to metallic iron drops evidence higher contents of fayalite molecule (Table 5). The enrichment is likely the effect of iron diffusion from hematite at the development of the reaction $Fe_2O_3 + 3Mg \rightarrow 3MgO + 2Fe$.

As quoted above, following a conventional hour lasting, step-heating treatment, enstatite can develop at 1000°C as breakdown product. Nonetheless, enstatite is lacking among our SHS products. The average reaction temperature above 1200°C, the repentine combustion and the high T gradients suggest the role of control (T) and kinetic (ΔT) factors during the recrystallization. It is likely that due to extremely high thermal gradients and high undercooling the growth of enstatite was not allowed.

5. Conclusions

Although a SHS reaction has been mostly addressed to metallic and metalloid materials, it resulted possible to obtain chemical-physical breakdown of a hydrous silicate such as chrysotile. The reaction is ignited by means of external heat sources for few seconds and proceeds as combustion wave through the reactants volume without any additional energy. In addition, secondary (industrial) minerals derive from the chrysotile breakdown.

As the mutagenic action of asbestos resides in habit, composition and size, neutralisation requires the structural change of the mineral fibre. All experiments demonstrated effective in destructing the fibrous habit of chrysotile, turning its composition to stubby olivine grains.

The SHS process in comparison with conventional thermal treatments, due to fast reaction time, low activation energy and simple instruments, particularly advantages the asbestos neutralisation, positively reflecting into time and costs of the process.

Finally, the product of this transformation is liable to be re-used for instance as abrasive, or refractory material: this represents the end of waste status and a second life as secondary raw material.

Acknowledgments

This work was carried in the frame of PRATT 2012 – UNIGE awarded to Laura Gaggero and of LIFE12 ENV/IT/000295 FIBERS (Coordinating beneficiary: University of Genoa). The authors acknowledge Claudio Belfortini for designing, crafting and acutely improving the SHS reaction chamber. Thanks are also due to Laura Negretti for help in mineral analyses acquisition.

References

1 H.I. Pass, D. Lott, F. Lonardo, M. Harbut, Z. Liu, A. Tang, M. Carbone, C. Webb, A. Wali, Asbestos exposure, pleural mesothelioma and serum osteopontin levels, N. Engl. J. Med., 353 (2005) 1564-1573.

2 Motion for a European Parliament Resolution on Asbestos related occupational health threats and prospects for abolishing all existing asbestos, 2012/2065(INI).

3 Y.M Chan, P. Agamuthu, R. Mahalingam, Solidification and stabilization of asbestos brake lining dust using polymeric resins, Env. Eng. Sci., 17, 4 (2000) 203–213.

4 A. F. Gualtieri, A solution for the full impregnation of asbestos: the use of an epoxy polymer resin, J. Appl. Poly. Sci., 75, 5 (2000) 713–720.

5 T. Sugama, R. Sabatini, L. Petrakis, Decomposition of chrysotile asbestos by fluorosulfonic acid, Ind. Eng. Chem. Res., 37 (1998) 79–88.

6 G. Gadikota, C. Natali, C. Boschi, A.H.A. Park, Morphological changes during enhanced carbonation of asbestos containing material and its comparison to magnesium silicate minerals, J. Hazard. Mater., 264 (2014) 42–52.

7 K. Anastasiadou , D. Axiotis, E. Gidarakos, Hydrothermal conversion of chrysotile asbestos using near supercritical conditions, J. Hazard. Mater., 179 (2010) 926–932.

8 A. Viani, A.F. Gualtieri, Recycling the product of thermal transformation of cement-asbestos for the preparation of calcium sulfoaluminate clinker, J. Hazard. Mater., 260 (2013) 813–818.

9 A. Averroes, H. Sekiguchi, K. Sakamoto, Treatment of airborne asbestos and asbestos-like microfiber particles using atmospheric microwave air plasma, J. Hazard. Mater., 195 (2011) 405–413.

10 F. Colangelo, R. Cioffi, M. Lavorgna, L. Verdolotti, L. De Stefano, Treatment and recycling of asbestos-cement containing waste, J. Hazard. Mater., 195 (2011) 391–397.

11 P. Plescia D. Gizzi, S. Benedetti, L. Camillucci, C. Fanizza, P. De Simone, F. Paglietti, Mechanochemical treatment to recycling asbestos-containing waste, Waste Manage., 23 (2003) 209–218.

12 A. Cattaneo, A.F. Gualtieri, G. Artioli, Kinetic study of the dehydroxylation of chrysotile asbestos with temperature by in situ XRPD, Phys. Chem. Minerals, 30 (2003) 177–183.

13 A.F. Gualtieri, A. Tartaglia, Thermal decomposition of asbestos and recycling in traditional ceramics, J. Eu. Ceram. Soc., 20 (2000) 1409–1418.

14 A.K. Datta, B.K. Samantaray, S. Bhattacherjee, Thermal transformation of chrysotile asbestos, Bull. Mater. Sci., 8 (1987) 497–503.

15 K.J.D. Mackenzie, H.R. Meinhold, Thermal reactions of chrysotile revisited: A ^{29}Si and ^{25}Mg MAS NMR study, Am. Mineral., 79 (1994) 43–50.

16 A.W. Naumann, W.H. Dresher, The influence of sample texture on chrysotile dehydroxylation, Am. Mineral., 51 (1966) 1200–1211.

17 N.L. Bowen, O.F. Tuttle, The system MgO-SiO_2-H_2O, Bull. Geol. Soc. Am., 60 (1949) 439–460

18 G.W. Brindley, J. Zussman, A structural study of the thermal transformation of serpentine minerals to forsterite, Am. Mineral., 42 (1957) 461–474.

19 C.J. Martin, The thermal decomposition of chrysotile, Miner. Mag., 41 (1977) 453–459.

20 M.C. Ball, H.F.W. Taylor, The dehydroxilation of chrysotile in air under hydrothermal conditions, Min. Mag., 33 (1963) 467–482.

21 G.W. Brindley, R. Hayami, Mechanism of formation of forsterite and enstatite from serpentine, Min. Mag., 35 (1965) 189–195.

22 A.G. Merzhanov, I.P. Boroviskaya, Self-propagating High-temperature Synthesis of refractory inorganic compounds, Dokl. Acad. Sci. USSR, 204 (1972) 429.

23 Z.A. Munir, Synthesis of high temperature materials by Self-Propagating Combustion methods, Amer. Ceram. Soc. Bull., 67 (1988) 342–349.

24 F. Maglia, U. Anselmi-Tamburini, S. Gennari, G. Spinolo, Dynamic behaviour and chemical mechanism in the self-propagating high-temperature reaction between Zr powders and oxygen gas, Phys. Chem. Chem. Phys., 3 (2001) 489-496

25 G. Cao, R. Orrù, Self-Propagating reactions for environmental protection: state of the art and future directions, Chem. L. Eng. J., 87, 2 (2002) 239-249

26 M. Porcu, R. Orrù, A. Cincotti, G. Cao, Self-propagating reactions for environmental protection: Treatment of wastes containing asbestos. Ind. Eng. Chem. Res., 44, 1 (2005) 85–91.

27 E. Isola, Approccio multiscala con metodologie integrate alle problematiche ambientali amianto–correlate. Tesi di Dottorato. Scuola di Dottorato di Scienze e Tecnologie per l'Ambiente e il Territorio, Università degli Studi di Genova, (2010) 195 pp.

28 E.J.W. Whittaker, F.J. Wicks, Chemical differences among the serpentinites "polymorphs": a discussion, Am. Mineral., 55 (1970) 1025–1047.

29 F.J. Wicks, A.G. Plant, Electron-microprobe and X-ray-microbeam studies of serpentine textures, Can. Mineral., 17 (1979) 785–830.

30 C. Viti, M. Mellini, Contrasting chemical compositions in associated lizardite and chrysotile in veins from Elba, Italy, Eur. J. Mineral., 9 (1997) 585–596.

31 C. Groppo, C. Rinaudo, D. Gastaldi, S. Cairo, R. Compagnoni, Micro-Raman spectroscopy for a quick and reliable identification of serpentine minerals from ultramafics, Eur. J. Mineral., 18 (2006) 319–329.

32 L. Gaggero, M. Ferretti, C. Belfortini, E. Isola, Metodo e apparato per l'inertizzazione di fibre di amianto, Italian Patent GE2010A000032 (2010).

33 J. Khorami, D. Choquette, F.M. Kimmerle, P.K. Gallagher, Interpretation of EGA and DTG analyses of chrysotile asbestos, Thermochim. Acta, 76 (1984) 87–96.

34 D.S. O'Hanley, Serpentinites: Records of tectonic and petrology history, Oxford University Press (1996) 277 pp

35 A.F. Gualtieri, C. Cavenati, I. Zanatto, M. Meloni, G. Elmi, M.L. Gualtieri, The transformation sequence of cement–asbestos slates up to 1200 °C and safe recycling of the reaction product in stoneware tile mixtures, J. Hazard. Mater., 152 (2008) 563–570.

Figure captions

Figure 1 – Chrysotile fibres extracted from a vein in serpentinite.

Figure 2 – A) Characterization by XRPD demonstrating the high purity of the phase. B) Micro-Raman spectrometry of starting material.

Figure 3 – XRPD patterns of chrysotile samples after 24 (A), 36 (B) and 48 (C) hours conventional thermal treatment in oven.

Figure 4 - SEM microphotographs of chrysotile bundles mixed with Mg and Fe oxide reagents and close up of the stratified chrysotile / reagents pellet. A) general view; B) insight of the intimate mixture obtained at 1,5 (t/m^2) pressure.

Figure 5 - Reaction chamber (open configuration): A) power supply; B) heated base; C) argon flow; D) sample; E) W coil; F) inspection window; G) closing cover.

Figure 6 - XRPD patterns of treated pellets, demonstrating the breakdown of chrysotile to Forsterite ($FeSiO_4$), Wustite (FeO) and Periclase (MgO). In particular, A and B refer to homogeneous pellets; C refers to the stratified pellet. D) Electron microprobe in situ analysis of Mg-rich olivine from treated samples. A slight increase in fayalite molecule occurs close to wustite grains.

Figure 7 - SEM Microphotograph of SHS treated pellets. The sample was stratified. A) Overall scoriaceous texture. B) Voids originated in the volatile release from chrysotile, surrounded by blocky, compositionally homogeneous forsterite. C) Irregular, swirly, amygdalar texture of bubble distribution, suggesting that volatile release occurred in a visco-plastic host material. D) Spongy texture defined by wustite shells enclosed in forsterite (light grey, arrow on the right side). E) subrounded granular wustite and periclase enclosed in massive forsterite patch. The concentration of granular wustite suggests blastesis along former discontinuities. F) Annealing of wustite grains.

Figure 8 - SHS reaction temperatures measured by a thermocouple on the sample, at increasing chrysotile concentrations.

FIGURE 1

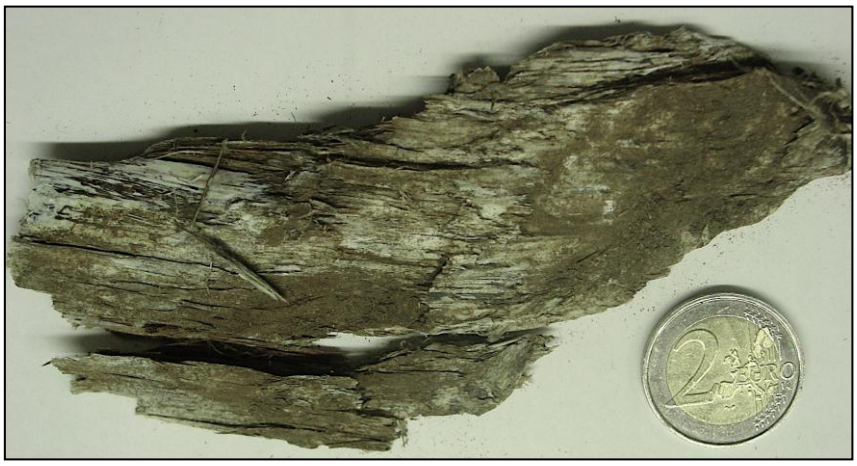

Chrysotile fibres extracted from a vein in serpentinite.

Figure 2

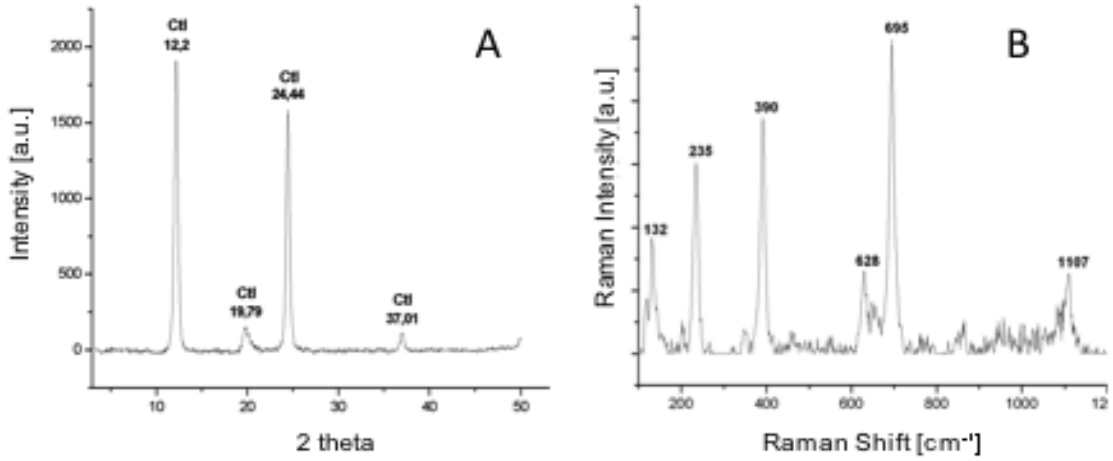

A) Characterization by XRPD demonstrating the high purity of the phase. B) Micro-Raman spectrometry of starting material.

Figure 3

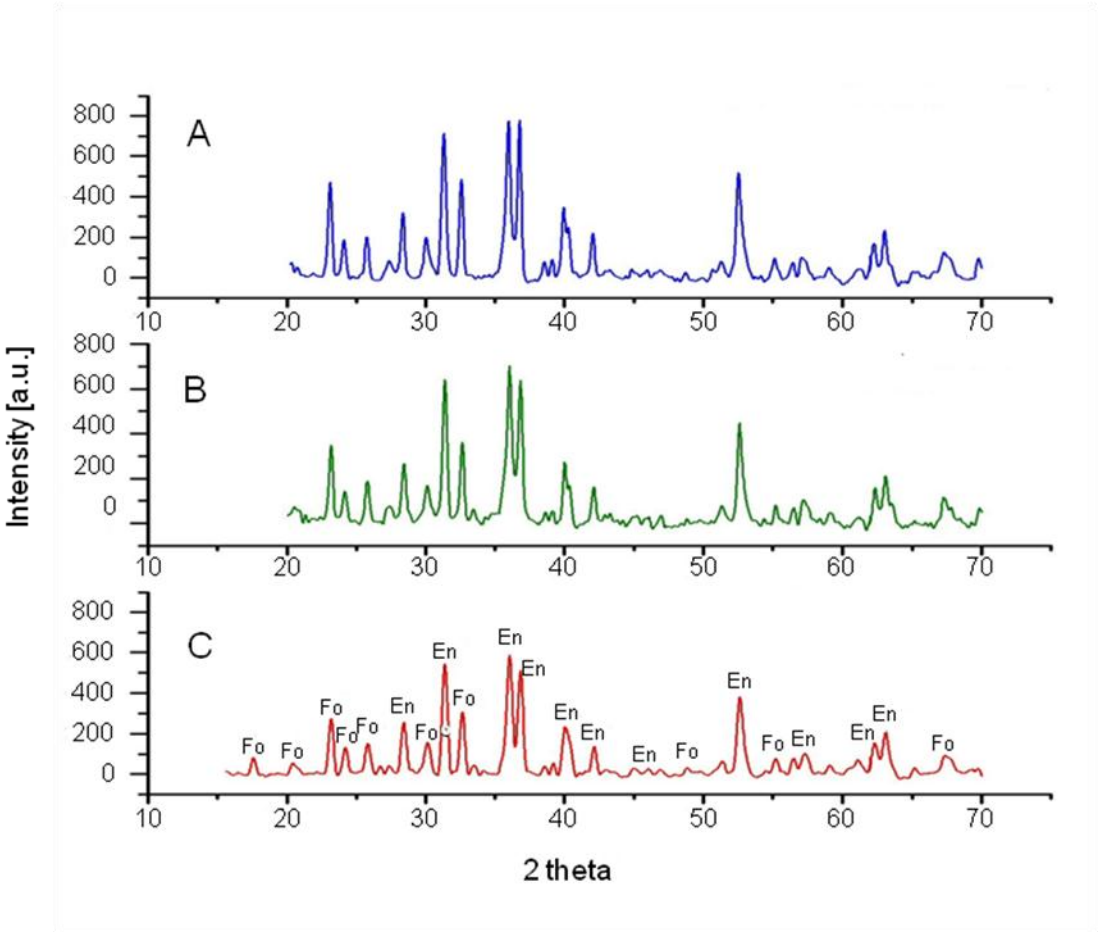

XRPD patterns of chrysotile samples after 24 (A), 36 (B) and 48 (C) hours conventional thermal treatment in oven.

Figure 4

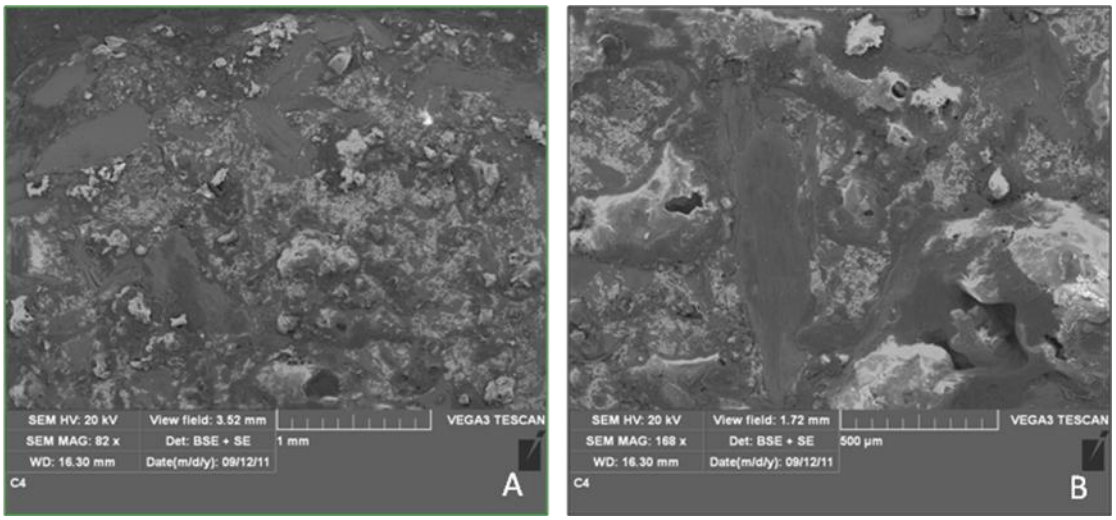

SEM microphotographs of chrysotile bundles mixed with Mg and Fe oxide reagents and close up of the stratified chrysotile / reagents pellet. A) general view; B) insight of the intimate mixture obtained at 1,5 (t/m^2) pressure.

Figure 5

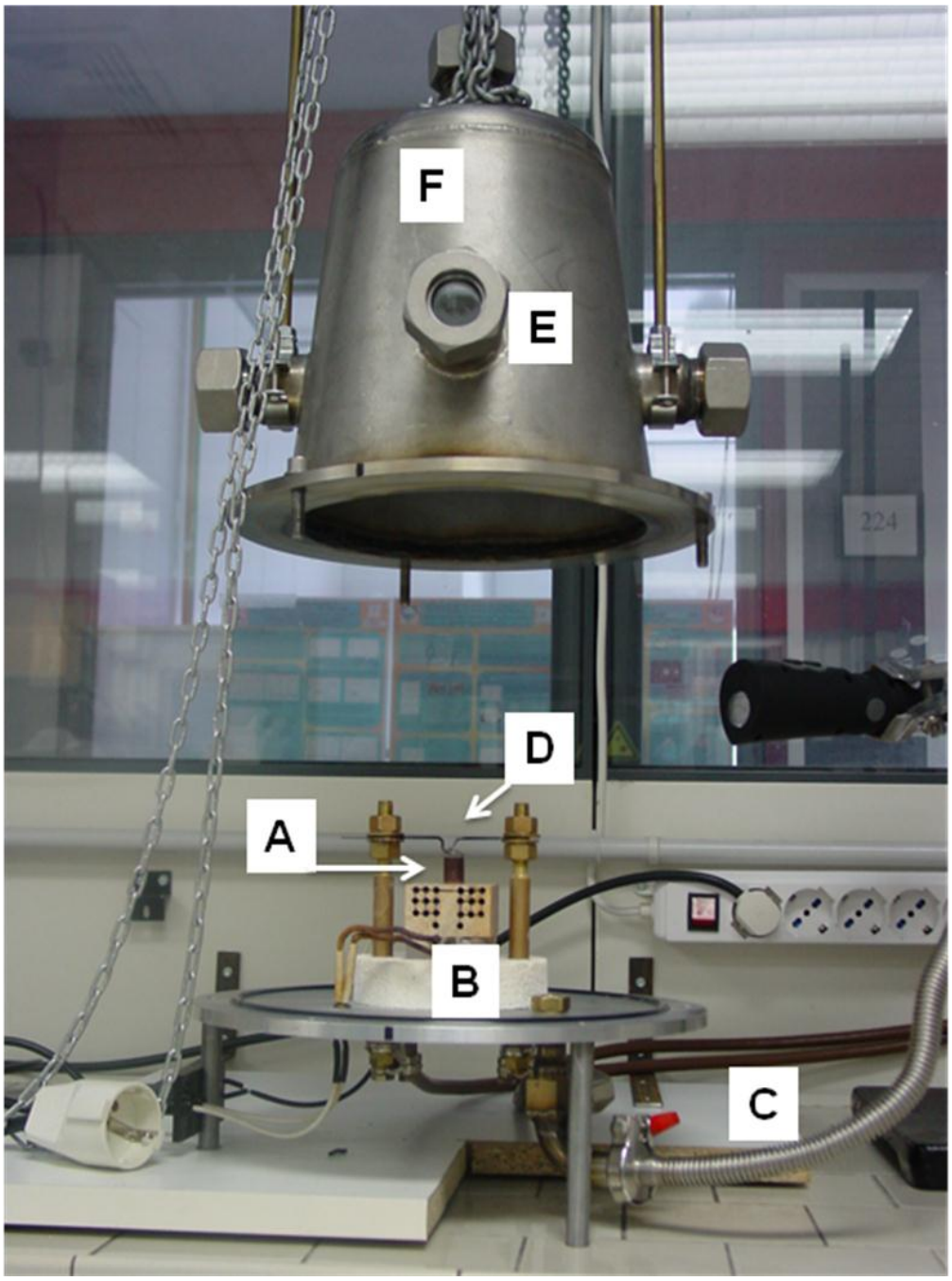

Reaction chamber (open configuration): A) sample; B) heated base; C) argon flow; D) W coil; E) inspection window; F) closing cover.

Figure 6

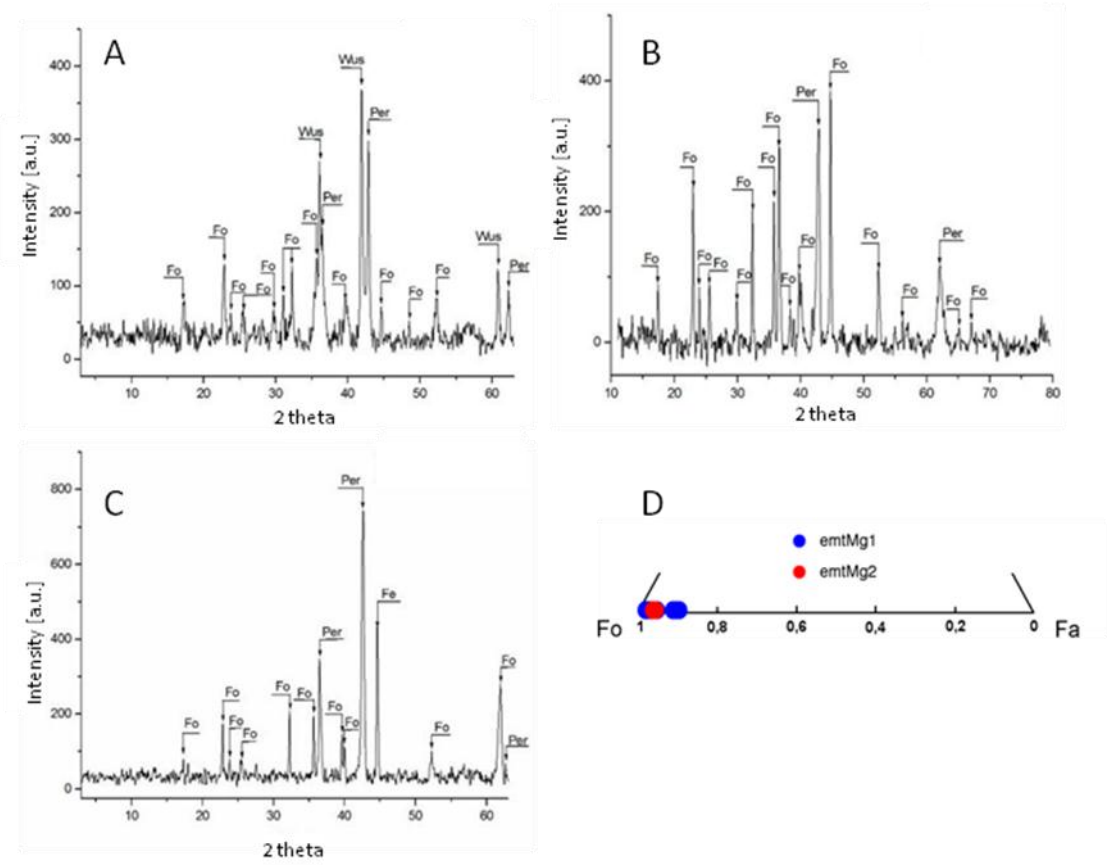

XRPD patterns of treated pellets, demonstrating the breakdown of chrysotile to Forsterite ($FeSiO_4$), Wustite (FeO) and Periclase (MgO). In particular, A and B refer to homogeneous pellets, C refers to the stratified pellet. D) Electron Microprobe in situ analysis of Mg-rich olivine from treated samples. A slight increase in fayalite molecule occurs close to wustite grains.

Figure 7

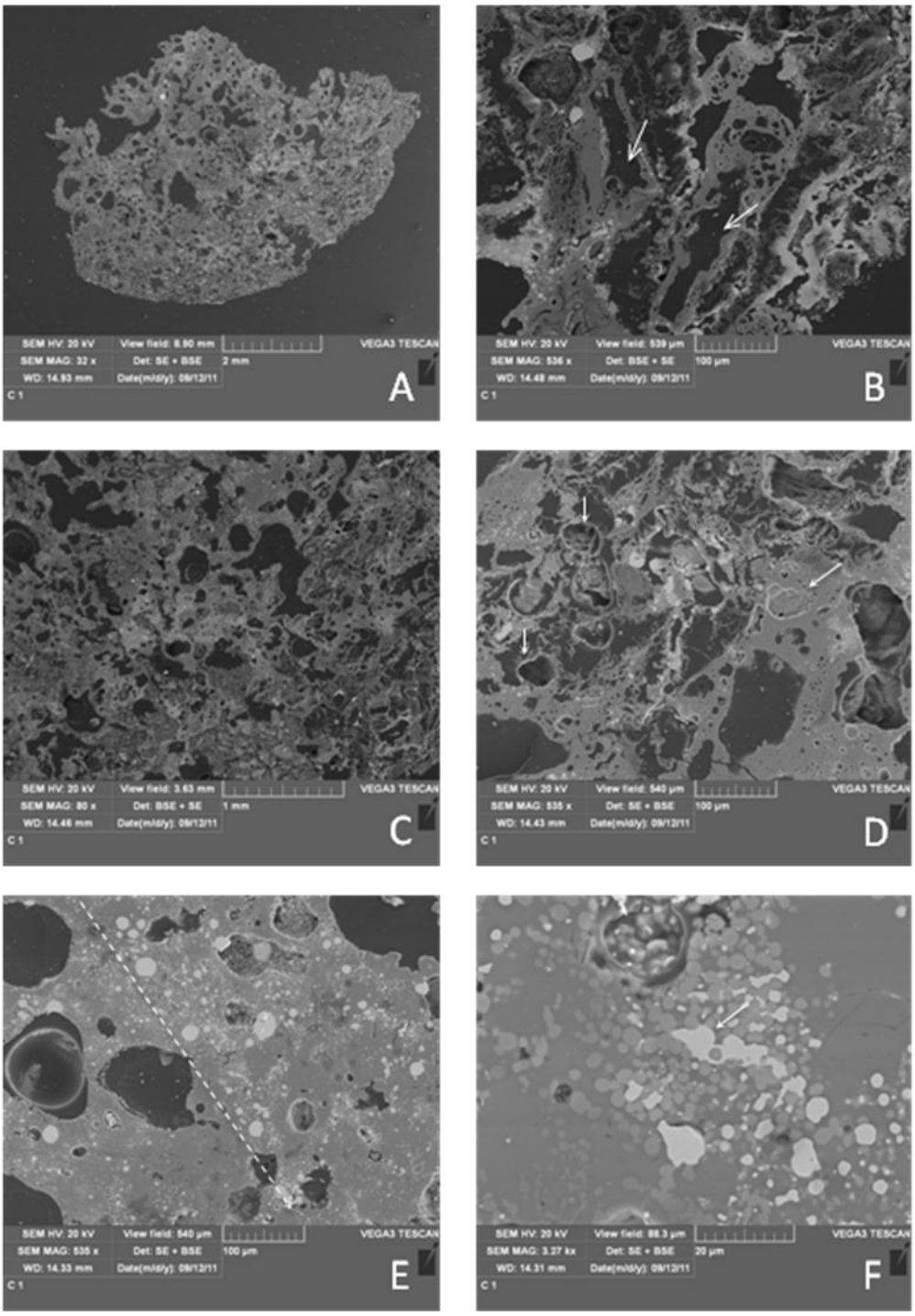

SEM Microphotograph of SHS treated pellets. A) overall scoriaceous texture. B) Voids originated in the volatile release from chrysotile, surrounded by blocky, compositionally homogeneous forsterite. C) irregular, swirly, amygdalar texture of bubble distribution, suggesting that volatile release occurred in a visco-plastic host material. D) Spongy texture defined by wustite shells enclosed in forsterite (light grey, arrow on the right side). E) subrounded granular wustite and periclase enclosed in massive forsterite patch. The concentration of granular wustite suggests blastesis along former discontinuities. F) Annealing of wustite grains.

Figure 8

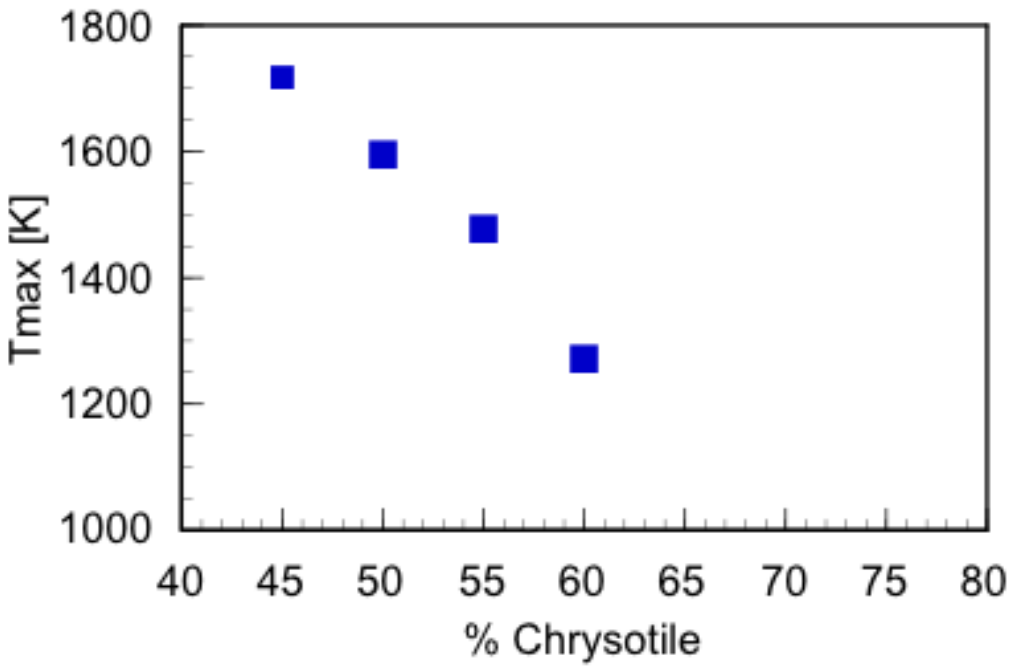

SHS reaction temperatures measured by a thermocouple on the sample, at increasing chrysotile concentrations.

Table captions

Table 1 - Representative EDS EMP analyses of the starting chrysotile form the Bargonasco vein.

Table 2 – Standard enthalpies of formation for reactants and mineral phases.

Table 3 - List of geometric features of chrysotile bundles in homogeneous pellets.

Table 4 – Reactants volume proportion, size and weight of the experimented ignited pellet series. Samples 1 – 4 contain stoichiometric amounts of reactants to provide the triggering of SHS and to obtain the forecast breakdown products. Chrysotile weight percent varies between 45 and 65. In samples 1 to 8 reactants are mixed, sample 9 was layered.

Table 5 - Representative in situ EDS composition of olivine obtained after SHS treatment. In isotropic, homogeneous pellets, Fo ranges between 90 and 98 moles %. In stratified pellet Fo is constantly 97-98 moles%. “Others” end-members in solid solution are Tephroite (Mn_2SiO_4) and Monticellite ($CaMgSiO_4$), with minor Cr end member.

Table 1

Cations	Chrysotile
Si	1.97 – 2.28
Al^{IV}	0.00 – 0.01
Al^{VI}	0.00 – 0.07
Mg	2.33 – 2.85
Fe	0.10 – 0.30

Representative EDS EMP analyses of the starting chrysotile form the Bargonasco vein.

Table 2

Reactant	ΔH_f [kJ/mol]	reference
$Mg_3Si_2O_5(OH)_4$ chrysotile	**-4353,0**	a
Mg_2SiO_4 forsterite	**-2170,4**	a
$MgSiO_3$ enstatite	**-1610,3**	a
MgO periclase	**-601,80**	a
Fe_2O_3 hematite	**-822,20**	b
Fe_3O_4 magnetite	**-1120,90**	c
$H_2O_{(g)}$	**-241,82**	c

a) US National Institute of Science and Technology

b) L. P. Ogorodova, I. A. Kiseleva, E. N. Korytkova, V. V. Gusarov, Calorimetric investigation of nanotubular hydrosilicates in the $Mg_3Si_2O_5(OH)_4$-$Ni_3Si_2O_5(OH)_4$ system, Glass Phys. Chem., 33, 4, (2007) 303-305

c) Di Svein Stølen, Tor Grande, Chemical Thermodynamics of Materials: Macroscopic and Microscopic Aspects, John Wiley & Sons Eds., (2003), 408 pp

Standard enthalpies of formation for reactants and mineral phases

Table 3

Chrysotile	
N° fibre bundles	452
average length of the single fiber	2831 μm
average surface	8493 μm^2
% area of chrysotile fibers	53.9%
% total area of chrysotile fibers	56.3%

List of geometric features of chrysotile bundles in homogeneous pellets.

Table 4

Sample #	Reactants	Chrysotile [weight %]	size [mm]		weight [g]
			Ø	**height**	
1	Fe_2O_3-Mg	51.90	10	7	0.96
2		54.37	13	7	1.91
3				8	1.96
4		54.37	13	13	2.87
5		45	13	7	1.87
6		50	13	7	1.95
7		60	13	7	1.96
8		65	13	7	1.96
9		50	10	7	0.69

Reactants volume proportion, size and weight of the experimented ignited pellet series Fe_2O_3-Mg. Samples 1 – 4 contain stoichiometric amounts of reactants to provide the triggering of SHS and to obtain the foreseen breakdown products. Chrysotile weight per cent varies between 45 and 65. In samples 1 to 8 reactants are mixed, sample 9 was layered.

Table 5

Pellet type	Homogeneous pellet													Stratified pellet				
Sample	EVIS1									EVIS2				EVIS1strati				
Oxide%	1	2	3	4	5	6	7	8	9	1	2	3	4	1	2	3	4	5
SiO_2	42,42	42,98	42,31	40,87	41,40	42,54	42,57	42,49	41,96	41,00	51,55	51,68	49,77	41,68	41,23	41,49	41,31	41,02
TiO_2	0,05	0,04	0,09	0,00	0,00	0,00	0,00	0,00	0,00	0,00	0,00	0,00	0,05	0,00	0,00	0,00	0,06	0,00
Al_2O_3	0,00	0,00	0,09	0,18	0,00	0,17	0,00	0,29	0,00	0,41	1,00	0,86	1,35	0,08	0,06	0,08	0,10	0,15
Cr_2O_3	0,00	0,05	0,07	0,00	0,00	0,09	0,07	0,00	0,05	0,04	0,12	0,09	0,05	0,09	0,10	0,10	0,11	0,00
FeO	2,20	2,03	1,79	9,39	8,04	1,29	1,81	2,06	4,36	8,80	2,73	3,61	3,18	2,63	2,06	2,64	1,64	2,44
MgO	55,19	54,78	55,53	49,49	50,37	55,82	55,27	55,05	53,63	49,68	46,34	43,48	47,25	55,97	56,26	56,13	56,79	56,40
MnO	0,10	0,07	0,00	0,00	0,07	0,00	0,14	0,05	0,00	0,04	0,00	0,14	0,07	0,09	0,06	0,00	0,00	0,00
NiO	0,00	0,00	0,00	0,00	0,00	0,00	0,00	0,00	0,00	0,00	0,00	0,00	0,00	0,00	0,00	0,00	0,00	0,00
CaO	0,05	0,05	0,10	0,04	0,07	0,05	0,09	0,06	0,00	0,03	0,06	0,08	0,00	0,06	0,09	0,06	0,11	0,06
Na_2O	0,00	0,00	0,00	0,00	0,00	0,00	0,00	0,00	0,00	0,00	0,00	0,00	0,00	0,00	0,00	0,00	0,00	0,00
K_2O	0,00	0,00	0,02	0,00	0,00	0,00	0,00	0,00	0,00	0,00	0,00	0,00	0,00	0,00	0,00	0,00	0,00	0,00
Total	100,01	100,00	100,00	99,97	99,95	99,96	99,95	100,00	100,00	100,00	101,80	99,94	101,72	100,60	99,86	100,50	100,12	100,07
N. of ions																		
Si	1,004	1,019	1,000	0,999	1,007	1,004	1,008	1,006	1,002	1,000	1,245	1,284	1,199	0,980	0,973	0,975	0,971	0,966
Ti	0,001	0,001	0,002	0,000	0,000	0,000	0,000	0,000	0,000	0,000	0,000	0,000	0,001	0,000	0,000	0,000	0,001	0,000
Al	0,000	0,000	0,003	0,005	0,000	0,005	0,000	0,008	0,000	0,012	0,029	0,025	0,038	0,002	0,002	0,002	0,003	0,004
Cr	0,000	0,001	0,001	0,000	0,000	0,002	0,001	0,000	0,001	0,001	0,002	0,002	0,001	0,002	0,002	0,002	0,002	0,000
Fe3	0,000	0,000	0,000	0,000	0,000	0,000	0,000	0,000	0,000	0,000	0,000	0,000	0,000	0,052	0,041	0,052	0,032	0,048
Fe2	0,044	0,040	0,035	0,192	0,164	0,026	0,036	0,041	0,087	0,180	0,055	0,075	0,064					
Mg	1,948	1,936	1,956	1,803	1,826	1,963	1,950	1,943	1,910	1,806	1,668	1,610	1,696	1,961	1,979	1,967	1,989	1,980
Mn	0,002	0,001	0,000	0,000	0,001	0,000	0,003	0,001	0,000	0,001	0,000	0,003	0,001	0,002	0,001	0,000	0,000	0,000
Ni	0,000	0,000	0,000	0,000	0,000	0,000	0,000	0,000	0,000	0,000	0,000	0,000	0,000	0,000	0,000	0,000	0,000	0,000
Ca	0,001	0,001	0,003	0,001	0,002	0,001	0,002	0,002	0,000	0,001	0,002	0,002	0,000	0,000	0,000	0,000	0,000	0,000
Na	0,000	0,000	0,000	0,000	0,000	0,000	0,000	0,000	0,000	0,000	0,000	0,000	0,000	0,000	0,000	0,000	0,000	0,000
K	0,000	0,000	0,001	0,000	0,000	0,000	0,000	0,000	0,000	0,000	0,000	0,000	0,000	0,000	0,000	0,000	0,000	0,000
Total	3,000	3,000	3,000	3,000	3,000	3,000	3,000	3,000	3,000	3,000	3,000	3,000	3,000	3,000	3,000	3,000	3,000	3,000
ENDMEMBERS																		
Forsterite	0,976	0,978	0,980	0,903	0,915	0,986	0,978	0,977	0,956	0,909	0,966	0,951	0,963	0,973	0,978	0,974	0,983	0,976
Fayalite	0,022	0,020	0,018	0,096	0,082	0,013	0,018	0,021	0,044	0,090	0,032	0,044	0,036	0,026	0,02	0,026	0,016	0,024
Others	0,002	0,002	0,002	0,001	0,003	0,001	0,003	0,003	0,000	0,001	0,002	0,004	0,001	0,002	0,002	0,001	0,001	0,001

Representative in situ EDS composition of olivine obtained after SHS treatment. In isotropic, homogeneous pellets, Fo ranges between 90 and 98 moles %. In stratified pellet Fo is constantly 97-98 moles%. “Others” end-members in solid solution are Tephroite (Mn_2SiO_4) and Monticellite ($CaMgSiO_4$), with minor Cr end member.